

# Sea Floor Classification with WorldView-2 and Bathymetry Data

H.M. Tulldahl <sup>a,\*</sup>, P. Philipson <sup>b</sup>, G. Tolt <sup>a</sup>

<sup>a</sup> Swedish Defence Research Agency, Box 1165, SE-581 11 Linköping, Sweden – (michael.tulldahl, gustav.tolt)@foi.se

<sup>b</sup> Vattenfall Power Consultant AB, Box 527, SE-162 16 Stockholm, Sweden – petra.philipson@vattenfall.com

**Abstract** – Earlier research results have shown some potential of using high resolution satellite data, like QuickBird, for sea floor classification, but the number of bands have been a limiting factor. In this paper we present the results of a preliminary study of the use of WorldView-2 data for benthic cover classification in the Swedish archipelago. WorldView-2 is the first high-resolution 8-band multispectral commercial satellite. We have explored the use of this better spectral resolution in combination with high-resolution depth data for mapping of sub-surface environments. Our results indicate that a method using high resolution imagery, preferably WV-2 or similar, together with bathymetry data can be used for sea floor classification in the Swedish archipelago. Our method includes atmospheric and water corrections of the satellite imagery. The corrected data are subsequently used for classification of the bottom.

**Keywords:** bathymetry, environment, lidar, vegetation

## 1 INTRODUCTION

The general purpose of the study is to develop remote sensing methods that can be efficient tools for investigations of large aquatic areas. In Sweden, large efforts are spent on environmental mapping and monitoring for the purpose of assessing ecosystem status and monitoring the fulfillment of national environmental goals and international agreements. However, there is still a lack of information for understanding ongoing changes in nature, as well as relationships between species and their habitats. Maps of sea bottom habitats are practically non-existent. Access to information about the extent, location and rate of change for different habitats is especially important in a time when anthropogenic influences are rapidly changing the environment.

The specific purpose of our study is evaluate a method using WorldView-2 image data together with high resolution depth data from airborne bathymetric lidar for classification of bottom vegetation and substrates. The lidar data is used for correction of the image for bottom depth and water turbidity. The corrected image data is used in classification tests with a classification model compiled from training data from field observations with underwater video. We compare the classification accuracy obtained with conventional (red, green) color bands to the result with an additional yellow band which is available in the WorldView-2 high-resolution satellite imagery. In this study we present our preliminary results from classification into five classes (Sand, Potamogeton, Filamentous algae, Fucus, and Soft sediment) within a small area of a WorldView-2 image.

## 2 METHODS

### 2.1 Test Site and Field Data

The investigated test site is located around Askö, an island in the archipelago 80 km south of Stockholm in the north-western Baltic Sea (Figure 1). The waters and archipelago around Askö is of scientific interest and Askö Laboratory – a centre for marine a marine field station belonging to Stockholm Marine Research Centre (SMF) is located on the island. The subsurface environment is diverse and rich in species. Valuable seabeds of pondweed (*Potamogeton perfoliatus*) and a large number of species varying in composition with respect to substrate can be found, as well as large areas of bladder wrack (*Fucus vesiculosus*) and sea clam.

Through off-line analysis of underwater video, together with GPS data, the abundance of species and other sea floor characteristics were estimated along several swaths in the area. The majority of the underwater video data were captured in May 2010.

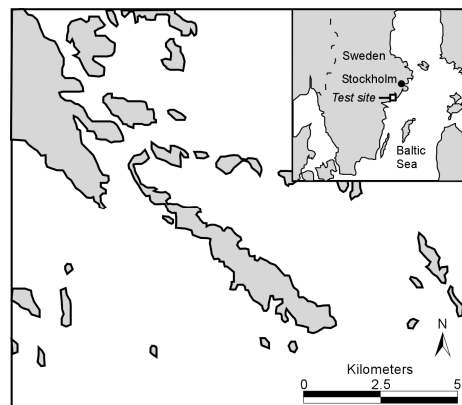


Figure 1. Test site in the Baltic on the east coast of Sweden (marked with a square in the inset figure).

### 2.2 Satellite Data

The WorldView-2 data used in the analysis was collected at 12:13 on the 2<sup>nd</sup> May 2010. WorldView-2 generates images with a spatial resolution of 0.5 m in panchromatic mode and 2.0 m in multispectral mode. Eight sensor bands are available; 4 standard colors: blue, green, red, near-IR 1 and 4 new colors: coastal, yellow, red edge, near-IR 2. In our study, we have used information from the multispectral bands 3, 4, and 5 (yellow, green, and red), which after an initial analysis were found to have useful signals down to about 5 m bottom depth while the other bands were strongly limited in depth range.

The image was geometrically corrected using 0.5-meter orthophotos as base reference and the derived RMSE was below pixel size. The image was then radiometrically calibrated, i.e. the raw numbers (DNs) have been converted to the top-of-atmosphere radiation, and atmospherically corrected using 6S

(Vermote et al., 1997). The output from 6S is ground reflectance and the atmospheric effects have been removed. Finally, a correction was made to reduce the effects of surface reflected skylight and solar glint. Earlier work has shown that this glint pattern, considerably make the analysis more difficult by blurring and concealing the appearance of the sea floor. By correcting for these effects a better representation of the bottom can be derived (Hochberg et al., 2003). An image based procedure to perform these corrections has been assembled by Claudia Giardino, CNR [Pers. Comm.] and were applied to the image. The algorithm uses the near infrared band to define the glint level and downwelling total irradiance and diffuse irradiance are estimated by the 6S code and used as input. The reflectance values for breaking waves and objects above surface are no longer valid after the correction. After the correction, the glint effects were decreased but not completely eliminated, reflectance values in the open water should thus be treated with caution. The output after the correction is the remote sensing reflectance

$$R_{rs}(\lambda) = L_w(\lambda) / E_d(\lambda). \quad (1)$$

where  $L_w(\lambda)$  is the upwelling radiance leaving the water and  $E_d(\lambda)$  the downwelling irradiance incident on the water for each wavelength band  $\lambda$ .

### 2.3 Lidar Data

The depth data used in the analysis were collected with the HawkEye II – Airborne coastal survey system (Airborne Hydrography AB, <http://www.airbornehydro.com>). The Hawk Eye II system surveys both land and sea floor simultaneously using two separate lasers emitting at wavelengths 1064 nm (NIR) for topography and at 532 nm (green) for bathymetry. The nominal flight altitude ranges from 250 m to 500 m and the swath width is between 100 m and 330 m. The bathymetric sounding spot density is between 0.1 and 0.35 soundings per  $m^2$ , and between 1 and 4 soundings per  $m^2$  for the topography lidar, both depending on flight altitude and swath width. Our work includes only the bathymetric data from the system.

Our results are based on lidar data from a survey in May 21, 2010. The maximum depth range of the lidar data was about 10 m. In the lidar data set, the depth data consisted of a point cloud with average point density of approximately 0.3 soundings per  $m^2$  corresponding to a horizontal distance of 1.8 m between each lidar data point. The lidar data was gridded and geometrically corrected to the same grid-scale as the corrected multispectral WorldView-2 image.

### 2.4 Correction for Water Depth and Turbidity

We have applied a method for correction of the WorldView-2 data using the bottom depth in each pixel. We write the remote sensing reflectance  $R_{RS}$  for each wavelength band  $\lambda$  as

$$R_{RS}(\lambda) = R_{RS}^b(\lambda) + R_{RS}^w(\lambda), \quad (2)$$

where  $R_{RS}^b(\lambda)$  and  $R_{RS}^w(\lambda)$  are the components reflected from the bottom and from backscattering from the water column respectively. We write the contribution from the bottom signal as

$$R_{RS}^b(\lambda) = \rho(\lambda) C_b \exp\{-D[\bar{K}_d(\lambda, D) + K_d(\lambda, \infty)]\} \quad (3)$$

where  $\rho(\lambda)$  is an estimate of the bottom reflectance,  $C_b$  a calibration factor,  $D$  the bottom depth,  $\bar{K}_d(\lambda, D)$  the vertically averaged downwelling diffuse attenuation coefficient from the water surface to depth  $D$ , and  $K_d(\lambda, \infty)$  the asymptotic diffuse attenuation coefficient. The calibration factor  $C_b$  can be used to calibrate to actual values of the bottom reflectance e.g. from field measurements of reflectance. Due to the scattering in water,  $K_d$  increases with depth which is an effect of the altered angular distribution of the downwelling light (Kirk, 1994). The increasing value of  $K_d$  levels off at that optical depth at which the asymptotic radiance distribution becomes established. We developed approximate equations for  $\bar{K}_d(\lambda, D)$  and  $K_d(\lambda, \infty)$  with numerical simulations using a lidar simulator (Tulldahl & Steinvall, 2004) to

$$\bar{K}_d(\lambda, D) = \frac{a(\lambda)}{\cos \theta_w} + D[0.032a(\lambda) - 0.0036] \quad (4)$$

for  $0 \text{ m} < D < 10 \text{ m}$ , and

$$K_d(\lambda, \infty) = 1.6a(\lambda) - 0.06, \quad (5)$$

where  $a(\lambda)$  is the absorption coefficient and  $\theta_w$  the subsurface solar zenith angle. The simulations which were the base for Eqs. (4) and (5) concern typical Baltic coastal water types (Steinval et al., 1994) with  $0.13 \text{ m}^{-1} < a < 0.35 \text{ m}^{-1}$ , and should be considered as preliminary models which require adjustments and improvements, e.g. for different water types with different scattering properties.

We estimate the contribution to  $R_{RS}$  from light reflected from the water column to

$$R_{RS}^w(\lambda) = b_b(\lambda) C_w \int_{z=0}^D \exp\{-D[\bar{K}_d(\lambda, z) + K_d(\lambda, \infty)]\} dz \quad (6)$$

where  $b_b$  is the water backscattering coefficient, and  $C_w$  a calibration coefficient which can be used e.g. for calibration against field measurements of the water optical properties. In our preliminary work, we have not yet compared estimates of the bottom reflectance or the water backscattering coefficient to field measurements of these parameters. Eq. (6) is further approximated to

$$R_{RS}^w(\lambda) \approx b_b C_w \left[ \frac{1 - \exp\{-D[\bar{K}_d(\lambda, D) + K_d(\lambda, \infty)]\}}{\bar{K}_d(\lambda, D) + K_d(\lambda, \infty)} \right] \quad (7)$$

for the case when  $\bar{K}_d(\lambda, D)$  is assumed to be a constant from the water surface ( $z = 0$ ) to the bottom depth  $D$ .

We developed an algorithm for inversion of WorldView-2 data and bottom depth to water optical parameters  $a$  and  $b_b$  and bottom reflectance  $\rho$  in the WorldView-2 multispectral bands (Bands 3-5). In brief, the algorithm tests numerical values for the parameters  $a$ ,  $b_b$ ,  $\rho$ , that minimize the RMS error

$$\varepsilon = \frac{1}{3n} \sum_{\substack{\lambda=3,4,5 \\ p=1,\dots,n}} \left[ (R_{RS})^2 - (R_{RS}^b + R_{RS}^w)^2 \right], \quad (8)$$

between the atmospherically corrected WorldView-2 remote sensing reflectance  $R_{RS}$  and the model for  $R_{RS}^b$  and  $R_{RS}^w$  according to Eqs. (3)-(5) and (7). The summation in Eq. (8) is taken over the wavelength bands  $\lambda$  and over spatially limited regions in the dataset, with each region having a total number  $n$  of pixels  $p$ . After the numerical estimation of the water optical parameters  $a(\lambda)$  and  $b_b(\lambda)$ , a manual fine-tuning of the parameters were made over regions in the image, and finally  $a(\lambda)$  and  $b_b(\lambda)$  for the whole test site were generated by interpolation from the estimated values in the selected regions. The correction of image data for water attenuation was then made pixelwise by solving the system of equations Eqs. (3)-(5) and (7) for  $\rho(\lambda)C_b$  using the estimated values of  $a(\lambda)$  and  $b_b(\lambda)$  and depth  $D$  from lidar data. The resulting water-corrected image thus contains estimated values which are proportional to the bottom reflectance in the WorldView-2 bands.

## 2.5 Classification

The corrected image data obtained with the methodology described above was subject to a classification analysis. Based on field data, five classes were defined: Sand (bare sand, cover 100 %), Potamogeton (*Potamogeton pectinatus* or *Potamogeton perfoliatus* > 75 %), Filamentous (mainly *Pilayella littoralis* > 75 %) Fucus (*Fucus vesiculosus* > 75 %), and Soft (soft sediment with < 25 % vegetation cover). A number of regions were selected in the image and used as training data. Figure 2 shows a scatter plot of water-corrected band intensities, i.e.  $\rho(\lambda)C_b$  in Eq. (3), for Bands 3-5 for each class. A quantitative measure of the separation of the clusters was performed by a test classification of the same (training) data, i.e. by internal evaluation of the classification accuracy. The data was modeled as a multivariate Gaussian distribution for each class, and a subsequent maximum likelihood (ML) classification was performed. The ML classification was achieved by allocating each pixel to its most likely class of membership.

## 3 RESULTS AND DISCUSSION

The resulting confusion matrix for water-corrected data using three sensor bands is shown in Table 1 and corresponds to an average User's Accuracy (UA) of 82 % and average Producer's Accuracy (PA) of 87 %. For comparison with a conventional image sensor (red, green, blue) we made a two-band classification test using only the red and the green bands (Bands 5 and 3). We recall that the blue band is of limited use in the Baltic water type. The resulting average accuracy for the two-band classification was 73 % (average UA) and 75 % (average PA). Most notably was the lower accuracy for the Potamogeton class which was evaluated to only 40 % (UA) for two-band classification, compared to 70 % for three bands. In the two-band classification, the Potamogeton class was mainly confused with the Filamentous class. The significantly better performance with three-band classification can be explained by the fact that the WorldView-2 yellow band (Band 4) increases the separation between these two classes (cf. Figure 2). Also, the Filamentous class gave significantly lower accuracy with a two-band classification accuracy of 66 % (UA) compared to 86 % for three bands. In the two-band classification, the Filamentous class was mainly confused with the Potamogeton class and to a smaller extent with the Fucus and Soft classes. The User's Accuracy for the Sand, Fucus, and Soft classes were similar or slightly lower (a few percent) in the three-band classification, compared to the results for two bands. The Producer's Accuracy for three-band classification were higher for all classes compared to two bands, except for Fucus where both three-band and two-band classification resulted in 87 % PA.

An example of a part of the test site is shown in Figure 3, where the image before (a) and after (b) water correction, and a classification map (c) are illustrated. The maximum bottom depth in this part of the test site is about 4 m. From a visual inspection of the classification result we note that the extent of the classes coincides with regions in the water-corrected image of similar spectral values. We also compared the classification result to a separate and independent field data set from ten locations within the classification map shown in Figure 3. Also this field data set was collected with underwater video, but by another field team. An overview of the comparison of the independent field data with the classification map is shown in Table 2. To the far right in the table, several classes are given within parenthesis if the field data point was situated on the border between different classes in the classification map. To the left in Table 2, the field data points for which the classification map (pixels) corresponds completely to the definition of the training classes (subsection 2.5) are marked with two stars (\*\*), and points which are partly corresponding are marked with one star (\*).

Table 1. Confusion matrix for internal evaluation using water-corrected image data from three bands (WorldView-2, Bands 3-5). The numbers in italics show the resulting number of pixels classified into each class.

	Class					
	Sand	Potamogeton	Filamentous	Fucus	Soft	PA (%)
Sand	25	<i>1</i>	<i>0</i>	<i>0</i>	<i>0</i>	96
Pota.	<i>0</i>	<i>14</i>	<i>1</i>	<i>0</i>	<i>0</i>	93
Filam.	<i>0</i>	<i>5</i>	<i>43</i>	<i>5</i>	<i>5</i>	74
Fucus	<i>0</i>	<i>0</i>	<i>3</i>	<i>20</i>	<i>0</i>	87
Soft	<i>0</i>	<i>0</i>	<i>3</i>	<i>0</i>	<i>14</i>	82
UA(%)	100	70	86	80	74	

Table 2. Comparison of field data from an independent field data set with the classification map shown in Figure 3. The classification is based on water-corrected WorldView-2 data, Bands 3-5.

Field data point No.	Field Data Substrate & Vegetation Cover (%)						WorldView-2 classification map
	Sand	Rock, Stone	Potamogeton	Fucus	Filamentous	Other	
1	55	45	30			<sup>a</sup>	Fucus
**2	5	95		70	20		Fucus
*3	80	20			20		Filamentous (Sand)
*4	98	2	15			<sup>b</sup>	Sand (Filamentous)
**5		100		100	10		Fucus
*6	85	15	65		15	<sup>c</sup>	Filamentous (Soft, Potamogeton)
*7	95	5		5			Sand
*8	25	80	10	80	30		Filamentous (Fucus, Potamogeton)
*9	100				10	<sup>d</sup>	Filamentous (Sand)
*10	15	85		50	50	<sup>e</sup>	Fucus

<sup>a</sup> *Chorda filum* 45 %, *Ruppia* 25 %

<sup>b</sup> *Ruppia* 15 %

<sup>c</sup> *Chorda filum* 10 %, *Ruppia* 10 %

<sup>d</sup> Decay 35 %

<sup>e</sup> *Chorda filum* 15 %

#### 4 CONCLUSIONS AND FURTHER WORK

We have tested a method for correction of WorldView-2 data for water depth and turbidity using high resolution depth data from airborne bathymetric lidar. The water corrected image data were used in classification tests with a classification model compiled from training data from field observations with underwater video. An internal evaluation with the training data indicates that the classification accuracy is significantly improved using the yellow channel in WorldView-2 data together with the red and green channels, compared to using only the standard colors (red and green channels). The resulting average user's accuracy for the two-band (red, green) classification was 73 % compared to 82 % for the three-band (red, yellow, green) classification. A comparison of our classification map in a small test area with an independent field data set shows relatively good correspondence.

Due to the small area investigated and the limited amount of independent field data in that area, we consider our results as preliminary. There are several interesting topics for future work, e.g. comparison of estimated bottom reflectance with field measurements of reflectance, further development of the water correction methods, and extension and evaluation of classification results for additional species/substrates and to larger areas. If large areas can be accurately classified, the method using high resolution satellite imagery and depth data can contribute with important information for environmental planning, monitoring, and for scientific purposes.

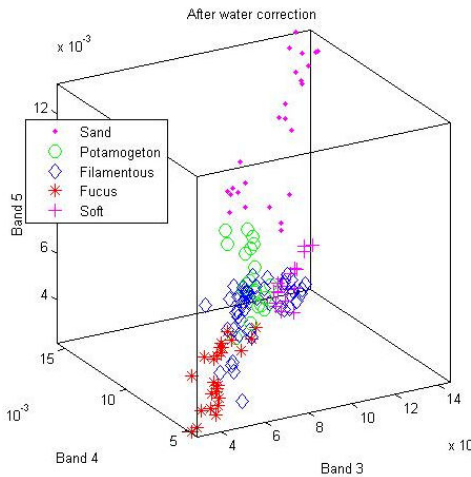


Figure 2. Scatter plots of water-corrected data for five classes for WorldView-2 Bands 3 (green), 4 (yellow), and 5 (red).

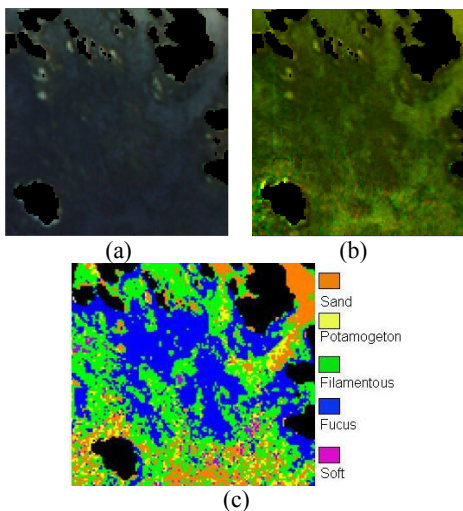


Figure 3. Image data (red, green and blue bands) before (a) and after (b) water correction, and the classification map (c). The size of the area is approximately 250 m  $\times$  250 m.

The result shows a relatively good correspondence for nine field points and incorrect results for Field point No. 1. One obvious explanation for the points with inaccurate or less accurate classification result is that all existing species are not covered within the five defined classes. An example is Field point No. 1 (Table 2), where the brown algae *Chorda filum* (Sea lace) were present with 45 % cover which may have contributed to the classification assignment to the Fucus class. In selecting the training data and defining the classes we restricted this preliminary analysis to species which were dominating and having high cover. Additionally, we focused on species/substrates which, in field data, had large spatial extent and thus was more easy to locate in the image data. Moreover, there are GPS position uncertainties in the field data, possibly up to a few meters, which may result in image pixels being selected as belonging to the wrong class. This effect is especially critical in sea floor environments where small patches of different species are mixed. The image data also contains intensity variations caused by shadowing effects on the sea floor, sun glints, and sea floor slopes, which add to the complexity of the problem and the classification performance.

#### ACKNOWLEDGEMENTS

This study was supported by the project "HISPARES - Spatial planning in archipelago waters by high spatial resolution remote sensing" financed by the European Union, Regional Development Fund, within the Central Baltic INTERREG IV A Programme 2007-2013. The authors gratefully acknowledge the University of Tartu, Estonia, Stockholm University, and AquaBiota Water Research AB for field data collection and interpretation, as well as the Swedish Environmental Protection Agency (EMMA-project) and Airborne Hydrography AB for cooperation concerning airborne lidar bathymetry data.

#### REFERENCES

- Hochberg, E. J., Andréfouët, S., and R.T., M. (2003). Sea surface correction of high spatial resolution IKONOS images to improve bottom mapping in near-shore environments. *IEEE Transactions on Geoscience and Remote Sensing* 41.
- Kirk, J. T. O. (1994). *Light and photosynthesis in aquatic ecosystems*. 2nd ed. Cambridge, UK: Cambridge U. Press.
- Steinvall, K. O., Koppari, K. R., and Karlsson, U. C. M. (1994). Airborne laser depth sounding. System aspects and performance. *Proceedings of Ocean Optics XII*, 2258, 392-412.
- Tulldahl, H. M. and Steinvall, K. O. (2004). Simulation of sea surface wave influence on small target detection with airborne laser depth sounding. *Appl. Opt.* 42, 2462-2483.
- Vermote, E. F., Tanré, D., Deuzé, J. L., Herman, M., and Morcrette, J. J. (1997). Second simulation of the satellite signal in the solar spectrum, 6S, an overview. *IEEE Transactions on Geoscience and Remote Sensing* 35, 675-686.